Kane-Fisher weak link physics in the clean scratched XY model

G. Lemarié,[1,2,*] I. Maccari,[3] and C. Castellani[2]

[1]*Laboratoire de Physique Théorique, IRSAMC, Université de Toulouse, CNRS, UPS, 31062 Toulouse, France*
[2]*Department of Physics, Sapienza University of Rome, P.le A. Moro 2, 00185 Rome, Italy*
[3]*ISC-CNR and Department of Physics, Sapienza University of Rome, P.le A. Moro 2, 00185 Rome, Italy*

The nature of the superfluid-insulator transition in one dimension has been much debated recently. In particular, to describe the strong disorder regime characterized by weak link proliferation, a scratched XY model has been proposed [New J. Phys. **18**, 045018 (2016)], where the transport is dominated by a single anomalously weak link and is governed by Kane-Fisher weak link physics. In this article, we consider the simplest problem to which the scratched XY model relates: a single weak link in an otherwise *clean* system, with an intensity J_W which decreases algebraically with the size of the system $J_W \sim L^{-\alpha}$. Using a renormalization group approach and a vortex energy argument, we describe the Kane-Fisher physics in this model and show that it leads to a transition from a transparent regime for $K > K_c$ to a perfect cut for $K < K_c$, with an adjustable $K_c = 1/(1-\alpha)$ depending on α. We check our theoretical predictions with Monte Carlo numerical simulations complemented by finite-size scaling. Our results clarify two important assumptions at the basis of the scratched XY scenario, the behaviors of the crossover length scale from weak link physics to transparency and of the superfluid stiffness.

I. INTRODUCTION

Understanding the effects of disorder on one-dimensional (1D) quantum Bosonic systems is a very challenging issue [1]. Without interactions, we know that even an infinitesimal degree of disorder leads to Anderson localization [2]. But what happens when interactions compete with disorder is much less clear. Theoretical studies in 1D [3,4] and higher dimensions [5] have shown that the competition between disorder and interaction leads to a superfluid-insulator transition. Understanding this transition is important because it is relevant for many different types of experimental systems, such as Josephson junction arrays [6], spin ladders [7], or cold atoms [8].

The nature of the superfluid-insulator transition has been much debated recently, with different scenarios put forward: a weak-disorder regime with a Berezinskii-Kosterlitz-Thouless (BKT) transition characterized by a jump of the Luttinger liquid parameter at the universal value $K_c = 3/2$ [3,4,9]; and a new strong disorder regime governed by weak link physics and a non-universal $K_c > 3/2$. In this strong disorder regime, a real-space renormalization group approach [10–13] and a "scratched XY model" incorporating a Kane-Fisher renormalization of weak links [14,15] have been proposed to describe the new properties of the superfluid-insulator transition.

More precisely, according to Refs. [10–13], the regime of strong disorder induces effectively a power-law distribution of weak links, which can be seen as abnormally weak Josephson couplings between superfluid puddles [16]. These weak links, denoted as J then have a power-law distribution $P(J) \sim J^\gamma$

and an effective model [10–13] suggests that the inverse of the superfluid density can be written as the average of the inverse weak link couplings $\rho_s^{-1} = \sum_i J_i^{-1}/L$ with L the system size. However, because the inverse weak links J_i^{-1} do not have a second moment for $\gamma \leqslant 1$, the central limit theorem does not apply [17]. On the contrary, the superfluid density may be dominated by the weakest link $J_{\min}$ over the L weak links. For power-law-distributed weak links, the weakest link scales as a power law with system size $J_{\min} \sim L^{-\alpha}$, with $\alpha = 1/(\gamma + 1)$. In this case, the superfluid density is predicted to vanish as $\rho_s \sim L^{\gamma/(\gamma+1)}$ for $\gamma < 0$, leading to an insulating state [13]. This is a very different mechanism, based on large disorder fluctuations rather than the proliferation of phase slips (see Ref. [18]) associated to the BKT transition in the weak disorder regime [1,3,4,9].

However, this argument does not take into account a possible Kane-Fisher renormalization of weak links (see Ref. [14]). Indeed, a striking prediction of Kane and Fisher [19,20] is that a weak link in an otherwise clean Luttinger liquid sees its effective strength $\mathcal{J}_W \sim J_W L^{-1/K}$ decrease with system size L so that the system is perfectly transparent $\rho_s \sim L\mathcal{J}_W \to 1$ when $K > 1$, whereas for $K < 1$, the weak link cuts the system in two, $\rho_s \to 0$. Kane-Fisher physics has important experimental consequences, e.g., for fractional quantum Hall edge states [21–24] and the delicate crossover it implies has been studied in different 1D quantum systems recently [25,26]. In Ref. [14], the authors proposed a scratched XY model where the transport in a given disordered sample of size L is dominated by the weakest link $J_{\min} \sim L^{-\alpha}$. They then suppose that Kane-Fisher physics applies to this situation, which should make the weakest link $J_{\min}$ weaker: $\mathcal{J}_{\min} \sim L^{-\alpha-1/K}$. Then $\rho_s \sim L^{1-\alpha-1/K}$ and a transition to an insulating phase is possible at $\alpha = 1 - 1/K_c < 1$, thus even for $\gamma > 0$ contrary to the previous analysis [10–13], with a critical value of the

Luttinger parameter $K_c = 1/(1 - \alpha)$ which can be larger than $3/2$ for $\alpha > 1/3$.

Despite several numerical studies [27–30], there is no consensus today on the strong disorder scenario. In particular, in Ref. [30], using extensive numerical simulations by the density matrix renormalization group and quantum Monte Carlo approaches, two different regimes of the BKT superfluid-insulator transition have been observed. At weak disorder, a Giamarchi-Schulz regime is observed where $K_c = 3/2$ and the superfluid density and the single particle correlator are self-averaging at criticality. On the contrary, the strong disorder regime is qualitatively different with a proliferation of weak links, $K_c > 3/2$ and self similar power-law critical distributions for the superfluid density and correlator characterized by the same exponent γ. While this work clearly validates a number of theoretical predictions made previously [4,13,14], it differs with the strong disorder scenarios of Refs. [13] and [14] on two important points. The critical values of γ have been found significantly larger than 0 ($\gamma > 2.3$), in contradiction with the strong disorder renormalization group approach [13], and the value of K_c is much larger than $1/(1 - \alpha)$ predicted by the scratched XY model [14].

To better understand the origin of these differences, we wanted to consider in detail, the simplest problem to which the scratched XY model [14] relates: a single weak link in an otherwise *clean* system, with an intensity J_W which decreases algebraically with the size of the system $J_W \sim L^{-\alpha}$. The predictions of Ref. [14] are indeed crucially based on the physics of this model, and in particular (i) on the existence of a characteristic length called "clutch scale," which describes the Kane-Fisher crossover physics, and (ii) on the assumption of a "classical flow" equation for the superfluid density. In Ref. [14], the clutch scale is derived from phenomenological arguments and the validity of the "classical flow" approximation used has not been checked. In this article, we shall give an analytical derivation of the clutch scale and of the crossover flow for the superfluid density which are then assessed by numerical simulations.

To describe the effect of a power-law weak link $J_W \sim L^{-\alpha}$ on a clean Luttinger liquid, we use the analogy between 1D quantum systems and the classical 1+1 XY model, where the additional dimension corresponds to the imaginary time in the quantum problem [1]. The two-dimensional (2D) XY model can be understood as an effective model describing the phase fluctuations associated to the 1D quantum case. Since the weak link potential term does not depend on the imaginary time in this analogy, the weak link is transposed into a vertical column of weak links (see Refs. [31–33] for the effect of 2D weak link disorder in the 2DXY model). By generalizing the Kane-Fisher analysis [19,20], we treat this problem analytically by a renormalization group approach within a self-consistent harmonic approximation, with the focus on the delicate crossover physics expected for this new model. We also perform numerical simulations by the classical Monte Carlo approach, complemented by finite-size scaling, to check carefully the analytical predictions. We further generalize the standard single vortex stability criterium to our power-law weak link case, by considering the electrostatic problem analogous to the scratched XY model, where the weak link column is replaced by a slab of diverging dielectric constant.

Our results confirm the key predictions of Ref. [14] in the case of a single weak link $J_W \sim L^{-\alpha}$ in a *clean* system, in particular that $K_c = 1/(1 - \alpha)$. Importantly, this allows us to characterize the Kane-Fisher transition in the classical 2DXY model. Indeed, a necessary condition for Kane-Fisher physics is that the bulk of the system is quasi-ordered, which in the classical 2DXY model requires $K > 2$ due to the Berezinskii-Kosterlitz-Thouless transition that arises at $K = 2$ toward a disordered phase [34–36]. By considering sufficiently large values of $\alpha > 0.5$, we can work in a regime where the threshold for the Kane-Fisher transition $K_c > 2$ and thus observe both the transparent and the cut regimes of Kane-Fisher physics.

The paper is organized as follows. In Sec. II, we describe the 2DXY model with a columnar weak link and the analytical and numerical approaches used to describe Kane-Fisher physics in this system. Section III describes the well known case of a constant weak link: we detail our renormalization group predictions for the evolution with system size of the effective weak link strength, and give in particular an analytical expression for the clutch scale assumed in Ref. [14]. We check these predictions with our numerical Monte Carlo results. In Sec. IV, we describe the evolution with system size of the stiffness, and assess numerically the "classical flow" assumed in Ref. [14]. Section V describes the new case of a power-law weak link whose strength decreases algebraically with system size. We show in particular that a Kane-Fisher transition can be observed in the 2DXY model at $K_c = 1/(1 - \alpha)$ for $\alpha > 0.5$. Section VI gives a complementary vortex energy argument for the Kane-Fisher transition at $K_c = 1/(1 - \alpha)$. Section VII discusses the implications of these results on the scratched XY scenario and concludes.

II. THE CLASSICAL 2DXY MODEL WITH A COLUMNAR WEAK LINK

A. Classical 2DXY model versus 1D quantum Bosonic systems

The classical 2DXY model consists of planar rotors of unit length on a two-dimensional lattice. The Hamiltonian is given by

$$H = -J \sum_{\langle i,j \rangle} \cos(\theta_i - \theta_j), \tag{1}$$

where J is the coupling constant, $\langle i, j \rangle$ denotes nearest neighbors on a square lattice of spacing set to $a = 1$, and θ_i is the angle of the rotor on site i with respect to some (arbitrary) direction in the two-dimensional vector space of the rotors.

At low temperature, statistical fluctuations involve only long-wavelength modes [34–37]. We can use a continuum approach, which means replacing the Hamiltonian of the classical 2DXY model by

$$\mathcal{H} = \frac{1}{2} J \int (\nabla \theta)^2 d\boldsymbol{r}. \tag{2}$$

Hence, we can understand the link between the classical 2DXY model and 1D quantum Bosonic systems [1]. One can write the partition function of the quantum system as a

classical field path integral:

$$Z = \int D\Psi(x,\tau)D\Psi^*(x,\tau)e^{-S/\hbar}, \tag{3}$$

where $\Psi(x,\tau)$ is a complex number field which depends both on x and τ the imaginary time. The field $\Psi(x,\tau) = \sqrt{\rho(x,\tau)}e^{i\theta(x,\tau)}$ can be written as a function of the density ρ and the phase θ. Usually, the superfluid to insulator transition is driven by phase fluctuations. In a low-energy, long-wavelength description, we can write an effective action [18,38] which describes the slow variations in the phase of the order parameter:

$$S_{\mathrm{eff}}[\theta] = \int dx\, d\tau \left[\frac{\rho_s}{2}(\partial_x\theta)^2 + \frac{\kappa}{2}(\partial_\tau\theta)^2 \right]. \tag{4}$$

Here ρ_s is the superfluid density and κ compressibility of the 1D quantum system. This action is equivalent to a $1+1$ classical XY model with the immaginary time direction replaced by the y direction. The so-called Luttinger parameter $K = \pi\sqrt{\rho_s\kappa}$ corresponds to $K = \pi J/T$ in the classical 2DXY model which controls the algebraic decay of the correlation function $\langle\cos(\theta_i - \theta_j)\rangle \sim r_{ij}^{-1/2K}$, where r_{ij} denotes the distance between the two sites i and j. In the classical 2DXY model, the Berezinskii-Kosterlitz-Thouless transition arises at the universal value $K = 2$.

B. Columnar weak link

We are interested in the 2D classical analog of a weak link in 1D quantum Bosonic systems. A weak link can be seen as an exponentially weak Josephson coupling between two superfluid systems, described by the following term:

$$H_W = -J_W\cos(\theta_L - \theta_R), \tag{5}$$

where $\theta_{L,R}$ is the phase at the left/right side of the weak coupling. In the mapping from 1D quantum to $1+1$ classical systems, an important property is that such potentials do not depend on immaginary time τ [1]. Therefore, the classical analog of the weak Josephson coupling Eq. (5) is a columnar weak link, translation invariant along y:

$$\mathcal{H}_W = -J_W \int dy \cos[\theta_L(y) - \theta_R(y)]. \tag{6}$$

In the discrete 2DXY model, this is equivalent to consider a column between say $x = 0$ and $x = 1$ with $J = J_W$ for all y, while $J = 1$ otherwise, and periodic boundary conditions along the x and y directions.

C. Analytical and numerical methods

In the following, we will describe the effect of a columnar weak link on the 2DXY model using two approaches. Analytical calculations are performed using, on the one hand, a perturbative renormalization group approach and a self-consistent harmonic approximation; on the other hand, a vortex energy argument. This is complemented by numerical simulations using a classical Monte Carlo method [39] similar to that used in Refs. [32,33], complemented by a finite-size scaling approach.

In the Monte Carlo approach we used, a single Monte Carlo step consists of five Metropolis spin flips of the whole lattice, needed to probe the correct canonical distribution of the system, followed by ten over-relaxation sweeps of all the spins, which help the thermalization leaving unchanged the energy (microcanonical spin sweep). For each temperature we perform up to $\sim 17 \times 10^4$ Monte Carlo steps, and we compute a given quantity averaging over the last 16×10^4 steps, discarding thus the transient regime which occurs in the first 10^4 steps (the Monte Carlo correlation time for the stiffness is less than 20 steps in the case of the largest system sizes $L = 256$ considered).

The two observables numerically computed are
(i) the superfluid stiffness ρ_s along the x axis:

$$\rho_s = \mathcal{J}_d - \mathcal{J}_p, \tag{7}$$

$$\mathcal{J}_d = \frac{1}{L}\left\langle \sum_{i=1}^{L} J_{i,i+x}\cos(\theta_i - \theta_{i+x}) \right\rangle, \tag{8}$$

$$\mathcal{J}_p = \frac{\beta}{L}\left\langle \left[\sum_{i=1}^{L} J_{i,i+x}\sin(\theta_i - \theta_{i+x})\right]^2 \right\rangle, \tag{9}$$

where $\langle\ldots\rangle$ stands for the average over the thermodynamical ensemble (the stiffness ρ_y along the y axis was computed using the previous formula with x replaced by y); (ii) the correlation function across the weak link:

$$C_W = \frac{1}{L}\left\langle \sum_{j=1}^{L} \cos(\theta_{L,j} - \theta_{R,j}) \right\rangle. \tag{10}$$

III. KANE-FISHER RENORMALIZATION OF A COLUMNAR WEAK LINK

Kane-Fisher physics [19,20] considers the transport through a single impurity/weak link in a 1D quantum system described by the Luttinger liquid theory, i.e., by an effective action such as Eq. (4) characterized by the Luttinger parameter $K = \pi\sqrt{\rho_s\kappa}$. In the noninteracting limit, corresponding to $K = 1$, it is well known that an incoming plane wave will be partially reflected and partially transmitted, with a transmission probability which is a nontrivial number between 0 and 1. On the contrary, Kane and Fisher showed that for an interacting 1D quantum system at the thermodynamic limit, the transmission is either perfect for $K > 1$ (i.e., for attractive interactions) or vanishes in the repulsive case $K < 1$. This physics has important experimental consequences, e.g., for fractional quantum Hall edge states [21–24].

The problem we are interested in concerns a power-law weak link whose strength J_W vanishes algebraically with system size. Before describing it, we will first consider the well known case of a constant weak link. Kane-Fisher physics has now been solved by nonperturbative [40,41] or exact [42] analytical methods, but we will resort here to a more standard perturbative renormalization group approach. We will compare our theoretical predictions with Monte Carlo numerical simulations.

The strategy we followed to describe the effect of a weak link on a column Eq. (6) in the 2DXY model was first (i) to study the relevance of Eq. (6) as a perturbation on a decoupled

system (corresponding to $J_W = 0$), and (ii) to describe the full crossover by taking into account J_W explicitly. Point (ii) will allow us to give an analytical expression for the clutch scale which describes the crossover physics as confirmed by our numerical results.

(i) Take a decoupled system described by the Hamiltonian Eq. (2) with open boundary condition along x (corresponding to $J_W = 0$). This condition implies no current along x at $x = 0$ thus $\frac{\partial \theta}{\partial x}|_{x=0} = 0$. We then use the standard identity for Gaussian distributed variables:

$$\langle \cos(\theta_R - \theta_L) \rangle = e^{-\frac{\langle (\theta_R - \theta_L)^2 \rangle}{2}}, \tag{11}$$

where R means $x = 0^+$ and L means $x = 0^- = L$. In the decoupled case, clearly $\langle \theta_R \theta_L \rangle = 0$. Moreover, the fluctuations of θ_R and θ_L are stronger than in the bulk because they lie at the boundary [1]. Indeed, the boundary condition $\frac{\partial \theta}{\partial x}|_{x=0} = 0$ implies that the usual Fourier decomposition performed to calculate $\langle \theta \theta \rangle$ has to be reformulated using $\cos(qx)$ instead of plane waves. After some calculations (see Ref. [43] for a detailed derivation), one finds that

$$\langle \theta_R \theta_R \rangle = \langle \theta_L \theta_L \rangle = 2 \langle \theta \theta \rangle_{\text{bulk}} = \frac{1}{K} \ln L, \tag{12}$$

with $K = \pi J / T$. Note that here and in the following, the system size L is dimensionless, measured as a function of a microscopic length scale a. Equations (11) and (12) imply that

$$\langle \cos(\theta_R - \theta_L) \rangle \sim L^{-1/K}. \tag{13}$$

At the open boundary, similarly to Luttinger liquids where the Lorentz invariance between space and time is broken [43], x and y are not equivalent. Indeed, the decay of correlations is controlled by the exponent $1/K$ at the boundary whereas it is the usual $1/(2K)$ in the bulk.

Finally, the RG flow of the weak link term Eq. (6) is obtained by assuming 1 as the bare dimension (corresponding to the rescaling of the variable y) and $\langle \cos(\theta_R - \theta_L) \rangle$ as the anomalous dimension:

$$\frac{dJ_W}{d\ell} = \left(1 - \frac{1}{K}\right) J_W, \tag{14}$$

with $\ell = \ln L$. The presence of the weak link term Eq. (6) is thus an irrelevant perturbation for $K < 1$: the weak link strength vanishes and cuts the system in two independent parts. On the contrary, it is a relevant perturbation for $K > 1$: According to this perturbative approach, the strength of the weak link J_W will be renormalized to larger and larger values. To be able to describe the crossover toward transparency, one needs, however, to go beyond this perturbation on a decoupled system.

(ii) Step (ii) thus attempts to evaluate Eq. (11) in the presence of J_W. We start by evaluating the propagator at gaussian level, i.e., the model we consider will be described by

$$\frac{1}{2} J \int_{L+R} (\nabla \theta)^2 d\mathbf{r} + \frac{1}{2} J_W \int_{x=0} [\theta_L(y) - \theta_R(y)]^2 \frac{dy}{a}. \tag{15}$$

This Gaussian approximation of the weak link coupling is intended to describe the saturation of the flow Eq. (14) at $J_W \approx 1$, i.e., a regime where the renormalized J_W is already large enough so that nonlinear effects in H_W Eq. (5) are negligible.

In the opposite limit of vanishing J_W, this approximation does not affect the flow Eq. (14) discussed above.

Let us first show how to approach the "pure" 1D model:

$$\frac{1}{2} J \int_{L+R} (\nabla \theta)^2 dx\, a + \frac{1}{2} J_W (\theta_L - \theta_R)^2. \tag{16}$$

We perform a Hubbard-Stratonovich decoupling of J_W in Eq. (16) introducing a variable λ:

$$e^{-\frac{1}{2T} J_W (\theta_L - \theta_R)^2} \propto \int d\lambda\, e^{-\frac{T}{2J_W} \lambda^2 + i\lambda(\theta_R - \theta_L)}. \tag{17}$$

In the following, we will denote $\tilde{J}_W = J_W / T$. Then at the action level, we can integrate out the θ degree of freedom obtaining $\frac{1}{2} \lambda^2 (G^0_{RR} + G^0_{LL})$, where G^0 is the local θ propagator with no J_W, from which

$$\langle \lambda \lambda \rangle = \left(\frac{1}{\tilde{J}_W} + W\right)^{-1} \text{ with } W = G^0_{RR} + G^0_{LL}. \tag{18}$$

Moreover, using Dyson equation, one can write $\langle \lambda \lambda \rangle = \langle \lambda \lambda \rangle_0 - \langle \lambda \lambda \rangle_0^2 G$ with $G = \langle (\theta_R - \theta_L)^2 \rangle$. From

$$\langle \lambda \lambda \rangle = \frac{\tilde{J}_W}{1 + \tilde{J}_W W} = \tilde{J}_W - \tilde{J}_W^2 G, \tag{19}$$

we get

$$G = \frac{1}{\tilde{J}_W} \left(1 - \frac{1}{1 + \tilde{J}_W W}\right) = \frac{W}{1 + \tilde{J}_W W}. \tag{20}$$

This equation corrects Eq. (11):

$$\langle \cos(\theta_R - \theta_L) \rangle = e^{-W/2} \rightarrow \langle \cos(\theta_R - \theta_L) \rangle = e^{-\frac{W}{2(1 + \tilde{J}_W W)}}. \tag{21}$$

Notice that $\frac{W}{2} = \frac{1}{K} \ln L$, Eq. (20) is therefore *not* what we want since Eq. (20) will always crossover toward $\frac{1}{\tilde{J}_W}$ irrespective of J_W.

The solution is to apply Eq. (16) really in 2D. This amounts to introduce a Hubbard-Stratonovich λ_ω for each Fourier component $\theta_{L,R}(\omega)$ (where ω is the wave vector associated to the direction y). Then, the second term in Eq. (15) is replaced by

$$\frac{1}{2\tilde{J}_W} \sum_\omega \lambda_\omega^2 - i \sum_\omega \lambda_\omega [\theta_L(\omega) - \theta_R(\omega)], \tag{22}$$

where we have taken advantage from translation invariance in the y-direction. The local propagator with no J_W is now replaced by $G^0_{RR}(\omega) = G^0_{LL}(\omega) = \frac{1}{K|\omega|}$ (i.e., the relevant singular part). Now Eq. (20) changes into

$$G(\omega) = \frac{W(\omega)}{1 + \tilde{J}_W W(\omega)} = \frac{2}{K} \frac{1}{|\omega| + 2\tilde{J}_W / K}. \tag{23}$$

Then the relevant exponent is

$$\frac{1}{2} \int_{1/L}^{1} d\omega\, G(\omega) \approx -\frac{1}{K} \ln \left(\frac{1}{L} + \frac{2\tilde{J}_W}{K}\right), \tag{24}$$

apart from an irrelevant constant. Therefore, in the presence of J_W, the correlation through the weak link should follow

$$\langle \cos(\theta_R - \theta_L) \rangle \propto L^{-1/K} \left(1 + \frac{2}{\pi} \frac{\mathcal{J}_W}{J} L\right)^{1/K}. \tag{25}$$
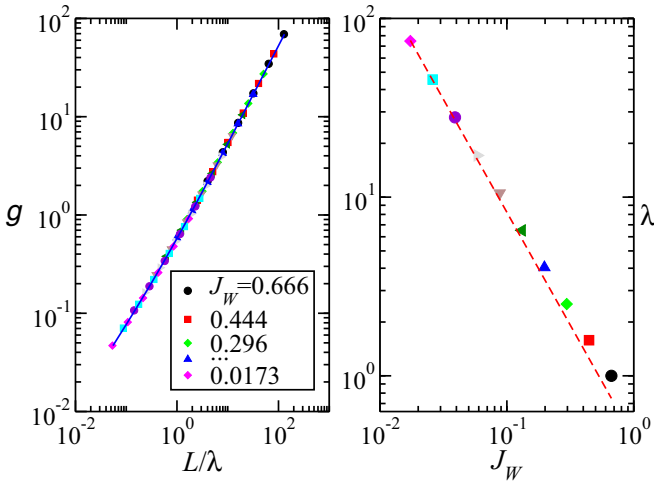
FIG. 1. Scaling behavior of the correlations across the weak link, characterized by the coupling $g = \frac{J_W}{J} L \langle \cos(\theta_R - \theta_L) \rangle$, for different system sizes L from 4 to 128 and different values of the weak link strength $J_W = 1.5^{-k}$ from $k = 1$ to $k = 10$. Left panel: When plotted as a function of L/λ, the data for the coupling g all collapse onto a single scaling curve. The blue line is a fit by the theoretical prediction Eq. (26) with $A_0 \approx 0.44$ and $A_1 \approx 4.1$. The crossover lengthscale λ is determined through finite-size scaling and is plotted on the right panel as a function of J_W. The red dashed curve shows the theoretical prediction Eq. (27). The 2DXY model with $J = 1$ and $T = 0.55$ has been considered, and the bulk value of $K \approx 4.8$ has been determined by the stiffness along the y axis, $K = \pi \rho_y / T$ at the largest system size $L = 128$.

In Eq. (25), $\mathcal{J}_W$ on the right-hand side is the renormalized effective strength of the weak link $\mathcal{J}_W = J_W \langle \cos(\theta_R - \theta_L) \rangle$. This approach can be understood as a self-consistent harmonic approximation [44], where, in the calculation of $\langle \cos(\theta_R - \theta_L) \rangle$, the original Hamiltonian Eq. (1) with a weak link Eq. (6) is replaced by an harmonic Eq. (15) with coupling J_W replaced by $\mathcal{J}_W$. We arrive thus at a self-consistent equation for the Kane-Fisher coupling:

$$g = \frac{J_W}{J} L \langle \cos(\theta_R - \theta_L) \rangle = A_0 \left(\frac{L}{\lambda} \right)^{\frac{K-1}{K}} (1 + A_1 g)^{1/K}. \quad (26)$$

A_0 and A_1 are two constants of order one which are difficult to determine theoretically. The crossover lengthscale is the so-called "clutch scale" of Ref. [14] and follows

$$\lambda \sim \left(\frac{J}{J_W} \right)^{K/(K-1)}. \quad (27)$$

We have tested these predictions with Monte Carlo simulations of the 2DXY model with a columnar weak link. Figure 1 represents the scaling behavior of the correlations across the weak link as a function of system size L for different values of the weak link strength J_W. When the data for the coupling g are plotted as a function of L/λ, they all collapse onto a single scaling curve which agrees very well with the theoretical prediction Eq. (26), as shown by the blue line. The crossover lengthscale λ, determined through finite-size scaling, depends only on J_W ($J = 1$ has a fixed value) and agrees very well with the theoretical prediction Eq. (27) (red dashed line).

IV. STIFFNESS

In this section, we want to describe the effect of the columnar weak link on the stiffness along the x axis. Due to the translation invariance along the y direction, a twist in the x-boundary conditions will not induce a current along the y axis, therefore we can consider this as a 1D problem. One can show [13] that the stiffness for a 1D chain of size L described by the harmonic action

$$S = \frac{1}{2} \sum_i J_i (\delta \theta_i)^2, \quad (28)$$

with $\delta \theta_i = \theta_{i+1} - \theta_i$, is given by

$$\frac{1}{\rho_s} = \frac{1}{L} \sum_i \frac{1}{J_i}. \quad (29)$$

Therefore, in the case of the 2DXY model with a columnar weak link, we may expect that

$$\frac{1}{\rho_s} = \frac{1}{L} \left(\frac{L-1}{J} + \frac{1}{J_W} \right). \quad (30)$$

Due to thermal fluctuations, the bulk stiffness is renormalized from J to ρ_y. Additionally, the weak link coupling strength J_W should be replaced by

$$\mathcal{J}_W = J_W \langle \cos(\theta_R - \theta_L) \rangle \quad (31)$$

through the Kane-Fisher RG flow described in the previous section. Incorporating these changes in Eq. (30) gives

$$\rho_s = \frac{\rho_y L \mathcal{J}_W}{L \mathcal{J}_W + \rho_y} = \frac{\rho_y g}{g + \rho_y}. \quad (32)$$

This (uncontrolled) approximation can again be understood as a self-consistent harmonic approximation [44], where the original Hamiltonian Eq. (1) with a weak link Eq. (6) is replaced by an harmonic Eq. (28) with couplings J replaced by ρ_y and J_W replaced by $\mathcal{J}_W$. Furthermore, Eq. (32) is justified by the fact that, in Kane-Fisher's physics, the weak link does not affect the properties of the bulk, i.e., it does not induce a change of ρ_y.

Figure 2 represents the evolution of the stiffness ρ_s as a function of system size L for different values of the weak link strength J_W. When the data are plotted as a function of L/λ, with $\lambda(J_W)$ the clutch scale, they collapse onto a single scaling curve which agrees very well with the theoretical Eq. (32) with the coupling g given by Eq. (26). The clutch scale λ depends only on J_W and has been determined through finite-size scaling. At small J_W, its behavior agrees well with the theoretical prediction Eq. (27). In Fig. 2, a flow toward transparency $\rho_s \to \rho_y$ is clearly observed, as expected for $K > 1$.

V. POWER-LAW WEAK LINK: ADJUSTABLE KANE-FISHER TRANSITION

Up to now, we have been able to investigate only the transparent regime of the Kane-Fisher transition which arises for $K > 1$. Indeed, in the 2DXY model, we are constrained to work at $K > 2$, otherwise the quasi long-range correlations are destroyed by the BKT transition [34–36]. Recently, Prokof'ev *et al.* proposed Ref. [14], in the context
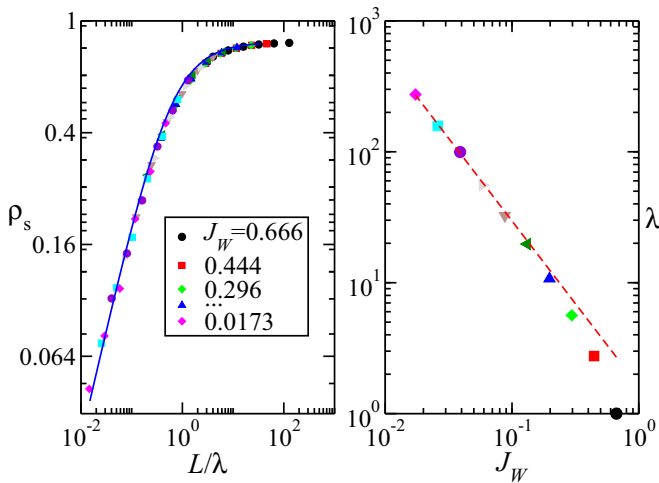
FIG. 2. Scaling behavior of the stiffness ρ_s along the x direction, as a function of system size and for different values of the weak link coupling $J_W = 1.5^{-k}$, with $k = 1$ to $k = 10$. Left panel: When plotted as a function of L/λ, the data for ρ_s collapse onto a single scaling curve well described by the theoretical prediction Eq. (32) (see the blue line). Right panel: The behavior of the clutch scale $\lambda(J_W)$, determined by finite-size scaling, is well described at small J_W by the theoretical prediction Eq. (27), as shown by the red dashed line. The system size varies from $L = 4$ to $L = 128$ and the temperature has been fixed to $T = 0.55$ ($J = 1$) so that $K \approx 4.8$, determined by the stiffness along the y direction at $L = 128$. The flow of the stiffness is toward transparency, $\rho_s \to \rho_y$, as expected for $K > 1$.

of the superfluid-insulator transition in 1D quantum disordered Bosons, that a weak link whose strength decreases algebraically with system size $J_W = J_0 L^{-\alpha}$, $\alpha > 0$, induces a Kane-Fisher transition [19,20] at a threshold $K_c = \frac{1}{1-\alpha} > 1$. In this section, we address this problem on the basis of our previous theoretical arguments and we show that it allows us to observe and characterize the Kane-Fisher transition in the 2DXY model.

A. Correlations across a power-law weak link

Let us now consider a power-law weak link $J_W = J_0 L^{-\alpha}$ and see how the theoretical predictions of Sec. III are modified. Inserting $J_W = J_0 L^{-\alpha}$ into Eq. (25) for the weak link correlations, we get a new self-consistent equation for the coupling $g = \frac{J_0}{J} L^{1-\alpha} \langle \cos(\theta_R - \theta_L) \rangle$:

$$g = A_0 \left(\frac{L}{\lambda}\right)^{\frac{K(1-\alpha)-1}{K}} (1 + A_1 g)^{1/K}, \tag{33}$$

with the clutch scale

$$\lambda \sim \left(\frac{J}{J_0}\right)^{\frac{K}{K(1-\alpha)-1}}. \tag{34}$$

Figure 3 represents this scaling behavior for $\alpha = 0.25$ and $T = 0.4$. When plotted as a function of L/λ, with λ the clutch scale given by Eq. (34), the data for the coupling g all collapse onto a single scaling curve which agrees well with the theoretical prediction Eq. (33), as shown by the blue line.
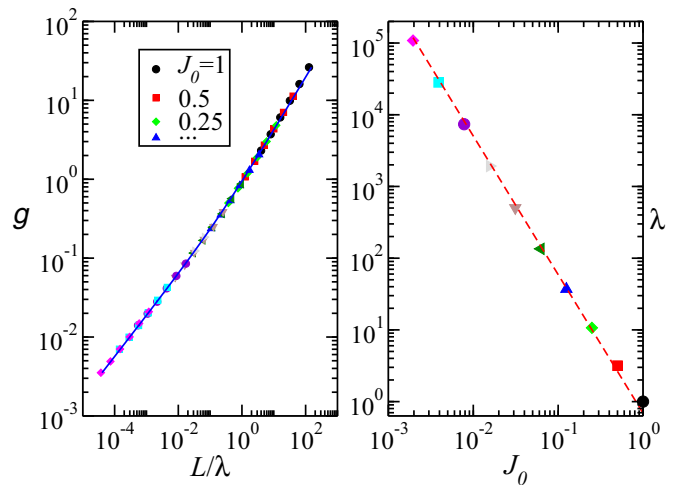

FIG. 3. Scaling behavior of the correlations across a power-law weak link $J_W = J_0 L^{-\alpha}$ as a function of system size and for different values of $J_0 = 2^{-k}$, from $k = 0$ to $k = 9$. Left panel: When the coupling $g = \frac{J_0}{J} L^{1-\alpha} \langle \cos(\theta_R - \theta_L) \rangle$ is plotted as a function of L/λ with λ the clutch scale which depends only on J_0, the data collapse onto a single scaling curve well fitted by Eq. (33) with $A_0 \approx 0.66$ and $A_1 \approx 3.9$, as shown by the blue line. Right panel: The behavior of the clutch scale λ, determined through finite-size scaling, as a function of J_0 is well fitted by Eq. (34), as shown by the red dashed line. The system size varies from $L = 4$ to $L = 128$. $\alpha = 0.25$, $T = 0.6$, and $J = 1$, so that $K = 4.3$, determined through the stiffness along the y axis.

B. Kane-Fisher transition on the stiffness

In this section, we show how a power-law weak link $J_W = J_0 L^{-\alpha}$ allows for the observation of the Kane-Fisher transition in the 2DXY model. According to Eqs. (32) and (33) the evolution of the stiffness as a function of system size depends on the variable L/λ with the clutch scale given by Eq. (34). This implies a Kane-Fisher transition at

$$K_c = \frac{1}{1-\alpha}. \tag{35}$$

If $K > K_c$, then the flow of the stiffness is toward transparency, while for $K < K_c$, the flow is toward a cut.

Setting $\alpha > 0.5$, we should be able to observe the Kane-Fisher transition in the 2DXY model since $K_c(\alpha) > 2$ is larger than the threshold of the BKT transition. Figure 4 shows the results in the case $\alpha = 0.75$ where $K_c(\alpha) = 4$ [see Eq. (35)]. For $T = 0.2$, $K \approx 14.9 > K_c$, we observe clearly that the stiffness converges toward its transparent value $\rho_s \to \rho_y$ as a scaling function of the variable L/λ. The agreement with the theoretical prediction Eq. (32) shown by the red dashed curve is excellent. Moreover, for $T = 0.8$, $K \approx 2.8 < K_c$, $K(1-\alpha) - 1 < 0$, and the flow is toward a cut. The data, when plotted as a function of L/λ, with λ given by Eq. (34), all collapse onto a single scaling curve given again by Eq. (32). This implies that the stiffness vanishes as a power law with system size $\rho_s \approx J_0 L^{\frac{K(1-\alpha)-1}{K}}$ at large L.

Close to the threshold $K \approx 4.3 \approx K_c$ for $T = 0.6$, Kane-Fisher renormalization of the weak link is almost absent, and the stiffness is a nontrivial number between 0 and ρ_y given by
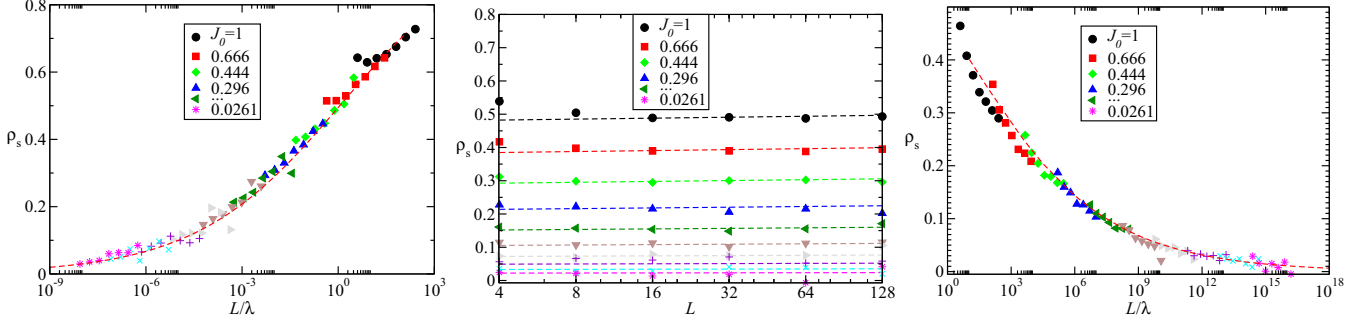
FIG. 4. Kane-Fisher transition on the 2DXY model with a power-law weak link $J_W = J_0 L^{-\alpha}$. $\alpha = 0.75$ implies a critical $K_c = \frac{1}{1-\alpha} = 4 > 2$ so that the Kane-Fisher transition from a flow toward transparency to a flow toward a cut can be observed in the quasiordered phase of the BKT transition $K > 2$. The left panel shows the data for $T = 0.2$ where $K \approx 14.9 > K_c$. When plotted as a function of L/λ with λ the clutch scale given by Eq. (34), the data collapse onto the scaling function Eq. (32) shown by the red dashed line. The right panel shows the case of $K \approx 2.8 < K_c$ ($T = 0.8$) where the flow is toward a cut $\rho_s \to 0$ when $L \gg \lambda$, and follows the theoretical prediction Eq. (32) (red dashed line). The middle panel corresponds to the vicinity of the Kane-Fisher transition, $K \approx 4.3 \approx K_c$ ($T = 0.6$) for which Kane-Fisher renormalization of the weak link is almost irrelevant and the stiffness depends only weakly on system size and follows again Eq. (32) (see the dashed lines). The values of $J_0 = 1.5^{-k}$ with $k = 0$ to $k = 9$, and the system size varies from $L = 4$ to $L = 256$ in the right and left panels and up to $L = 128$ in the middle panel.

Eq. (32), a prediction that agrees well with the numerical data (see the dashed lines in the middle panel).

VI. VORTEX ENERGY ARGUMENT

This final section aims at giving a thermodynamical argument for the adjustable $K_c = 1/(1-\alpha)$ of the Kane-Fisher transition in the case of a power-law weak link. It is well-known that the BKT transition is driven by topological vortex excitations [34–36]. The original argument for the BKT transition [35] compares the energy cost of a single vortex excitation with its entropy, which are both found to scale logarithmically with system size in two dimensions, so that the free energy reads $F = E - TS = (\pi J - 2T)\ln L$. For $K = \pi J/T > 2$, we have a proliferation of single vortices and the quasi long-range order is destroyed. A similar argument can be made for the Kane-Fisher transition in 1D quantum systems [18], where vortices in the x, τ plane (τ being the imaginary time) are then constrained to locate only in the vicinity of the columnar weak link. This constraint changes the entropy per vortex to $S = \ln L$ since there are only L different configurations of the vortex, instead of L^2. We thus recover the threshold $K_c = 1$ for the standard Kane-Fisher transition. It is, however, not clear how to extend these ideas to the case of a power-law weak link. As we will show, the energy of a single vortex in the case of a power-law weak link depends in a nontrivial manner on α and L and this allows us to recover $K_c = 1/(1-\alpha)$ for the threshold of the Kane-Fisher transition in this case.

The issue is to evaluate the energy of a single vortex in a configuration which consists in a slice B of width $2d$ with coupling J_W between two L^2 systems A and A' with coupling J, with $J_W/J \equiv W \ll 1$. For simplicity, the vortex is supposed to be located in the middle of B. We first use the standard analogy with an electrostatic problem (see, for example, Ref. [37]). The vortex is characterized by the circulation

$$\oint_{\mathcal{C}} \nabla\theta \cdot d\boldsymbol{l} = \int_{\mathcal{S}} (\nabla \times \boldsymbol{j}_\perp) = 2\pi, \qquad (36)$$

where the current field $\boldsymbol{j}_\perp = \nabla\theta$. We introduce the scalar function Φ such that $\boldsymbol{j}_\perp = \nabla \times (\hat{z}\Phi) = (\partial_y\Phi, -\partial_x\Phi, 0)$. Therefore, $\nabla \times \boldsymbol{j}_\perp = (0, 0, -\nabla^2\Phi)$, i.e., Φ satisfies the Poisson equation:

$$\nabla^2\Phi = -2\pi\delta(\boldsymbol{r}). \qquad (37)$$

In the following, we denote by $\boldsymbol{D} = -\nabla\Phi$. The conditions at the boundary are

$$JD_y^A = J_W D_y^B, \qquad (38)$$

$$D_x^A = D_x^B, \qquad (39)$$

which express the current conservation $(J_{x,y}\nabla_{x,y}\theta)_A = (J_{x,y}\nabla_{x,y}\theta)_B$ with $(J_x)_A = J$ and $(J_x)_B = J_W$, while $J_y = J$ everywhere. Thus, this problem is equivalent to a dielectric problem with $\boldsymbol{D}$ interpreted as the electric displacement field, $1/J(\boldsymbol{r})$ the analog of the permittivity and $\boldsymbol{E} = J\boldsymbol{D}$ the analog of the electric field.

In the Appendix, we derive the explicit form of the electric displacement field through the method of image charges. The energy is then evaluated as

$$E_{\text{vort}} = \frac{1}{2}\int_{A+B} J(\boldsymbol{r})\boldsymbol{D}(\boldsymbol{r})^2 d\boldsymbol{r} \approx \frac{1}{2}\int_A J(\boldsymbol{r})\boldsymbol{D}(\boldsymbol{r})^2 d\boldsymbol{r}. \qquad (40)$$

The result is that for a constant weak link J_W,

$$E_{\text{vort}} \approx J \ln L. \qquad (41)$$

The entropy of such a vortex constrained on a slice B is $\ln L$; therefore, the Kane-Fisher transition appends when the energy and entropy terms compensate exactly, i.e., at $\pi J = T$, or $K_c = 1$. However, for $J_W = J_0 L^{-\alpha}$, we find (see the Appendix)

$$E_{\text{vort}} \approx J \ln(L^{1-\alpha}), \qquad (42)$$

leading to $K_c = \frac{1}{1-\alpha}$ in the case of a power-law weak link.

VII. CONCLUSION

In this paper, we have studied a simple model underlying the scratched XY scenario [14] for the strong disorder regime of the 1D superfluid-insulator transition [3,4,9–15,27–30]. The model consists of a weak link whose strength decreases algebraically with the system size $J_W \sim L^{-\alpha}$, in an otherwise *clean* system. Using the analogy between 1D quantum systems and the classical 2DXY model, where the weak link is replaced by a weak link column, we were able to describe a Kane-Fisher transition [19,20] from a transparent regime for $K > K_c$ to a perfect cut for $K < K_c$, with an adjustable $K_c = 1/(1 - \alpha)$ depending on α. Our theory is found in very good agreement with the results of Monte Carlo numerical simulations and accounts for the full crossover from weak link physics to transparency.

This work clarifies two important assumptions at the basis of the scratched XY scenario [14]. First, the "clutch scale," describing the crossover of the superfluid density, is given by Eq. (34), and second the validity of the "classical flow," i.e., Eq. (32), has been checked with numerical data (see Figs. 2 and 4). Importantly, the coupling $g = \frac{J_0}{J} L^{1-\alpha} \langle \cos(\theta_R - \theta_L) \rangle$ is the analog of the variable $1/w$, Eq. (2.13) of Ref. [14]. From our Eq. (33), the logarithmic derivative of the coupling g with respect to L follows:

$$\frac{\partial g}{\partial \ln L} = \frac{K(1 - \alpha) - 1}{K - gA1/(1 + A1g)} g, \qquad (43)$$

which corrects the renormalization flow for w, Eq. (2.21c) of Ref. [14], with $\zeta = 1 - \alpha$. Notice that in our Eq. (43), the denominator varies from K at small g (i.e., $L \ll \lambda$) to $K - 1$ at large g ($L \gg \lambda$), contrary to Eq. (2.21c) of Ref. [14], where it is always $K - 1$.

While our results validate several predictions made in Ref. [14], the Kane-Fisher transition that we find is clearly distinct from a BKT transition such as the 1D superfluid-insulator transition. In particular, the stiffness in the cut regime $K < K_c$ decreases as a power law with system size instead of the exponential decay characteristic of the insulating phase. Moreover, at the transition, we do not observe the strong (logarithmic) finite-size effects expected for a BKT transition, but the stiffness stays constant as a function of system size and depends crucially on the microscopic strength of the weak link (see the middle panel of Fig. 4).

In fact, the scratched XY model [14] incorporates another important ingredient: the bulk of the system should not be considered clean, but instead incorporates the effect of many weak links. In Ref. [14], the authors propose that such a bulk can be described by a clean bulk with a renormalized coupling $J(L)$ accounting for the other weak links self-consistently. We stress that this is an uncontrolled assumption which has not been tested yet. In Ref. [26], the effect of a weak link in a disordered XXZ chain was studied. It was argued, in the presence of bond-disorder, that a weak link is healed even in the antiferromagnetic case (where $K < 1$), in contrast to the clean bulk case where healing occurs only in the ferromagnetic case ($K > 1$). Moreover, the corresponding clutch scale has a logarithmic dependency on the weak link strength which is very different from the algebraic dependence found

here [Eq. (34)]. More work is therefore needed to describe the Kane-Fisher physics in the presence of a disordered bulk.

As a final remark, let us discuss the recent numerical study [15] of the scratched XY model with power-law-distributed weak links. In the regime where the arguments of Ref. [14] predict a transition, the numerical results of Ref. [15] show very strong finite-size effects which practically prevent to distinguish the insulating behavior from the superfluid one with the available systems sizes (as large as $L = 512$). It is well known that BKT transitions have strong logarithmic finite-size corrections at criticality, and their precise knowledge is important to characterize numerically the critical behavior (see, e.g., Ref. [45]). In Ref. [14], the authors have made such a prediction, however based on the assumptions already discussed concerning the clutch scale, the classical flow and the self-consistent bulk. Our theory has clarified the first two assumptions and in particular corrects the renormalization flow of g [Eq. (43)]. If the strong-disorder scenario based on the scratched XY model is valid, this may change the logarithmic corrections at criticality and thus the critical value of the disorder strength. It would be interesting to extend our approach to the case of a power-law weak link in a disordered bulk, in particular to assess the relevance of the interplay between different weak links in providing the insulating behavior.

APPENDIX: ENERGY OF A VORTEX

1. Electric displacement field through the method of image charges

In this Appendix, we describe first how to find the D field defined by

$$\nabla D = 2\pi \delta(\boldsymbol{r}),$$

with the boundary conditions described by Eq. (38). The simplest way is to use the method of image charges and to put the origin (0,0) at the right interface [the vortex is in $(-d, 0)$]. B is described by charges α_n with $\alpha_0 = 1$ in $(-d, 0)$, $n > 0$ in $\boldsymbol{r}_n = (-d - 2nd, 0)$, and $n < 0$ in $\boldsymbol{r}_n = (-d + 2|n|d, 0)$. The symmetry implies $\alpha_n = \alpha_{-n}$ (it is the complication as compared to the case of a single interface). A (i.e., the domain $x < -2d$ is described by charges $\beta_n, n \leqslant 0$, in $\boldsymbol{r}_n$, and A' ($x > 0$) by charges $\beta_n, n \geqslant 0$ in $\boldsymbol{r}_n$. Note that α_n and α_{-n-1} (and β_n) have singularities $[(x - d - 2nd)^2 + y^2]^{-1}$ and $[(x - d + (2|n| + 2)d)^2 + y^2]^{-1}$, which have the same dependence in y at the interface $x = 0$ (at the right interface: $[d^2(1 + 2nd)^2 +$

$y^2]^{-1}$ and $[(1 + 2|n|)^2 d^2 + y^2]^{-1}$). There are two equations to consider:

$$WD_y^B = D_y^A, \tag{A1}$$

$$D_x^B = D_x^A, \tag{A2}$$

with $W = J_W/J$ which involve $(\alpha_0, \alpha_{-1}, \beta_0),..., (\alpha_n, \alpha_{-n-1}, \beta_n)$. Using $D_x = y/[(x - r_n)^2 + y^2]$ and $D_y = (x - r_n)/[(x - r_n)^2 + y^2]$, we get

$$W(\alpha_n y + \alpha_{-n-1} y) = \beta_n y, \tag{A3}$$

$$\alpha_n r_n + \alpha_{-n-1} r_{-n-1} = \beta_n r_n. \tag{A4}$$

At this point, d has disappeared (it will appear in the UV cutoff $d \geqslant a$):

$$\alpha_n + \alpha_{-n-1} = W^{-1} \beta_n, \tag{A5}$$

$$-\alpha_n(1 + 2n) + (1 + 2n)\alpha_{-n-1} = -\beta_n(1 + 2n), \tag{A6}$$

thus,

$$\alpha_n + \alpha_{-n-1} = W^{-1} \beta_n, \tag{A7}$$

$$\alpha_n - \alpha_{-n-1} = \beta_n. \tag{A8}$$

The solutions are

$$\alpha_n = (W^{-1} + 1)\frac{\beta_n}{2}, \tag{A9}$$

$$\alpha_{-n-1} = (W^{-1} - 1)\frac{\beta_n}{2}, \tag{A10}$$

which we rewrite as

$$\beta_n = 2\alpha_n \frac{W}{1 + W}, \tag{A11}$$

$$(\alpha_{n+1} \equiv) \quad \alpha_{-n-1} = \alpha_n \frac{1 - W}{1 + W}. \tag{A12}$$

With $\alpha_0 = 1$,

$$\alpha_n = \left(\frac{1 - W}{1 + W}\right)^n, \tag{A13}$$

$$\beta_n = 2\frac{W}{1 + W}\left(\frac{1 - W}{1 + W}\right)^n. \tag{A14}$$

(1) For $W = 1$ (i.e., $J_W = J$) we have $\alpha_0 = \beta_0 = 1$ and $\alpha_n = \beta_n = 0$ for $n \geqslant 1$.

(2) $W = 0$, $\alpha_n = 1$, and $\beta_n = 0$ (the field is entirely confined in B).

(3) $W \ll 1$, $\alpha_n \approx (1 - 2W)^n$ and $\beta_n = 2W(1 - W)(1 - 2W)^n$.

Finally, the field in A is

$$\boldsymbol{D}_A(\boldsymbol{r}) = \sum_{n \geqslant 0} \beta_n \frac{\boldsymbol{r} - \boldsymbol{r}_n}{|\boldsymbol{r} - \boldsymbol{r}_n|^2} = \sum_{n \geqslant 0} \beta_n \frac{[x + d(2n + 1), y]}{(x + d(2n + 1))^2 + y^2}, \tag{A15}$$

with

$$\beta_n = \frac{2W}{1 + W}\left(\frac{1 - W}{1 + W}\right)^n. \tag{A16}$$

2. Electrostatic potential energy

The second step is now to evaluate

$$\frac{1}{2}J \int_A d\boldsymbol{r}\, \boldsymbol{D}_A^2(\boldsymbol{r}).$$

a. Singular and regular terms

A direct evaluation of the sum involved in $\boldsymbol{D}_A$ is difficult. Instead, one approximation that we can make is the following:

$$\boldsymbol{D}_A \approx \sum_{n < n_c} \beta_n \frac{\boldsymbol{r}}{r^2} + \sum_{n \geqslant n_c} \beta_n \frac{-\boldsymbol{r}_n}{r_n^2}, \tag{A17}$$

where $n_c = r/(2d)$ such that $n \ll n_c \Leftrightarrow |\boldsymbol{r}_n| \ll |\boldsymbol{r}|$. The idea is that

$$\boldsymbol{D}_{\text{sing}} \equiv \sum_{n < r/(2d)} \beta_n \frac{\boldsymbol{r}}{r^2} = \frac{2W}{1 + W} \sum_{n < r/(2d)} p^n \frac{\boldsymbol{r}}{r^2}$$

$$= (1 - p^{r/(2d)})\frac{\boldsymbol{r}}{r^2} \tag{A18}$$

is the important term with respect to $D_{\text{reg}}\hat{x}/d$ with

$$D_{\text{reg}} \equiv \frac{2W}{1 + W} \sum_{n \geqslant r/(2d)} p^n \frac{1}{2n + 1}. \tag{A19}$$

In the previous equations, $p = (1 - W)/(1 + W)$.

b. Regular term

The D_{reg} term can be evaluated as follows:

$$D_{\text{reg}} = \frac{2W}{1 + W}\frac{1}{\sqrt{p}}\sum_{n \geqslant r/(2d)} \frac{\sqrt{p}^{2n+1}}{2n + 1}$$

$$= \frac{W}{1 + W}\frac{1}{\sqrt{p}}\sum_{n > r/(2d)} \frac{p^n}{n}. \tag{A20}$$

Let us denote $I_n \equiv \sum_{k \geqslant 0}^n p^k$. It is clear that

$$J_n = \sum_{k \geqslant 0}^n \frac{p^{k+1}}{k + 1} = \int_0^p I_n\, dp'. \tag{A21}$$

Since $I_n = \frac{1 - p^{n+1}}{1 - p}$,

$$J_n = -\ln(1 - p) - \int_0^p \frac{p'^{n+1}}{1 - p'}dp', \tag{A22}$$

where the first term on the right-hand side is J_∞,

$$\sum_{n > r/(2d)} \frac{\sqrt{p}^n}{n} = J_\infty - J_{r/(2d)-1} = \int_0^p \frac{p'^{r/(2d)}}{1 - p'}dp'. \tag{A23}$$

Using $p \approx 1 - 2W \approx 1 - 2J_0 L^{-\alpha}$, we can rewrite the previous integral as

$$\int_0^p \frac{p'^{r/(2d)}}{1 - p'}dp' = \int_{2J_0 L^{-\alpha}}^1 \frac{(1 - u)^{r/(2d)}}{u}du. \tag{A24}$$

$(1 - u)^{r/(2d)} \approx 0$ for $u \gg 2d/r$, while ≈ 1 for $u \ll 2d/r$, therefore we can approximate the last integral as

$$\int_{2J_0 L^{-\alpha}}^{1} \frac{(1-u)^{r/(2d)}}{u} du \approx \int_{2J_0 L^{-\alpha}}^{2d/r} \frac{1}{u} du = \ln\left(\frac{L^{\alpha} d}{r J_0}\right). \quad (A25)$$

Finally,

$$D_{\text{reg}} \approx W \ln\left(\frac{L^{\alpha} d}{r J_0}\right) \approx J_0 L^{-\alpha} \ln\left(\frac{L^{\alpha} d}{r J_0}\right). \quad (A26)$$

c. Vortex energy

The vortex energy is therefore given by the singular part:

$$E_{\text{vort}} \approx \frac{1}{2} J \int_A d\mathbf{r}\, D_{\text{sing}}^2(\mathbf{r}) \approx \int_d^L (1 - p^{r/(2d)}) \frac{1}{r} dr. \quad (A27)$$

We have

$$p^{r/(2d)} \approx (1 - 2W)^{r/(2d)} \approx (1 - 2J_0 L^{-\alpha})^{r/(2d)} \approx e^{-rJ_0/(dL^{\alpha})}. \quad (A28)$$

Therefore,

$$\text{for } r \gg L^{\alpha} d/J_0, \ p^{r/(2d)} \approx 0, \quad (A29)$$

$$\text{while for } r \ll L^{\alpha} d/J_0, \ p^{r/(2d)} \approx 1. \quad (A30)$$

Hence, the integral Eq. (A27) can be approximated by

$$E_{\text{vort}} \approx \int_{L^{\alpha} d/J_0}^{L} \frac{1}{r} dr = \ln\left(\frac{L J_0}{L^{\alpha} d}\right) = (1 - \alpha) \ln L + \text{cste.} \quad (A31)$$

[1] T. Giamarchi, *Quantum Physics in One Dimension*, Vol. 121 (Oxford University Press, Oxford, 2004).

[2] P. W. Anderson, Phys. Rev. **109**, 1492 (1958).

[3] T. Giamarchi and H. J. Schulz, Europhys. Lett. **3**, 1287 (1987).

[4] T. Giamarchi and H. J. Schulz, Phys. Rev. B **37**, 325 (1988).

[5] M. P. A. Fisher, P. B. Weichman, G. Grinstein, and D. S. Fisher, Phys. Rev. B **40**, 546 (1989).

[6] K. Cedergren, R. Ackroyd, S. Kafanov, N. Vogt, A. Shnirman, and T. Duty, Phys. Rev. Lett. **119**, 167701 (2017).

[7] M. Klanjšek, H. Mayaffre, C. Berthier, M. Horvatić, B. Chiari, O. Piovesana, P. Bouillot, C. Kollath, E. Orignac, R. Citro, and T. Giamarchi, Phys. Rev. Lett. **101**, 137207 (2008).

[8] C. D'Errico, E. Lucioni, L. Tanzi, L. Gori, G. Roux, I. P. McCulloch, T. Giamarchi, M. Inguscio, and G. Modugno, Phys. Rev. Lett. **113**, 095301 (2014).

[9] Z. Ristivojevic, A. Petković, P. Le Doussal, and T. Giamarchi, Phys. Rev. Lett. **109**, 026402 (2012).

[10] E. Altman, Y. Kafri, A. Polkovnikov, and G. Refael, Phys. Rev. Lett. **93**, 150402 (2004).

[11] E. Altman, Y. Kafri, A. Polkovnikov, and G. Refael, Phys. Rev. Lett. **100**, 170402 (2008).

[12] E. Altman, Y. Kafri, A. Polkovnikov, and G. Refael, Phys. Rev. B **81**, 174528 (2010).

[13] G. Refael and E. Altman, C. R. Phys. **14**, 725 (2013).

[14] Z. Yao, L. Pollet, N. Prokof'ev, and B. Svistunov, New J. Phys. **18**, 045018 (2016).

[15] T. Pfeffer, Z. Yao, and L. Pollet, arXiv:1807.09184.

[16] R. Vosk and E. Altman, Phys. Rev. B **85**, 024531 (2012).

[17] J.-P. Bouchaud and A. Georges, Phys. Rep. **195**, 127 (1990).

[18] V. A. Kashurnikov, A. I. Podlivaev, N. V. Prokof'ev, and B. V. Svistunov, Phys. Rev. B **53**, 13091 (1996).

[19] C. L. Kane and M. P. A. Fisher, Phys. Rev. Lett. **68**, 1220 (1992).

[20] C. L. Kane and M. P. A. Fisher, Phys. Rev. B **46**, 15233 (1992).

[21] K. Moon, H. Yi, C. L. Kane, S. M. Girvin, and M. P. A. Fisher, Phys. Rev. Lett. **71**, 4381 (1993).

[22] P. Fendley, A. W. W. Ludwig, and H. Saleur, Phys. Rev. Lett. **74**, 3005 (1995).

[23] L. Saminadayar, D. C. Glattli, Y. Jin, and B. Etienne, Phys. Rev. Lett. **79**, 2526 (1997).

[24] R. De Picciotto, M. Reznikov, M. Heiblum, V. Umansky, G. Bunin, and D. Mahalu, Nature (London) **389**, 162 (1997).

[25] R. Vasseur, J. L. Jacobsen, and H. Saleur, Phys. Rev. Lett. **112**, 106601 (2014).

[26] R. Vasseur, A. Roshani, S. Haas, and H. Saleur, Europhys. Lett. **119**, 50004 (2017).

[27] S. Pielawa and E. Altman, Phys. Rev. B **88**, 224201 (2013).

[28] F. Hrahsheh and T. Vojta, Phys. Rev. Lett. **109**, 265303 (2012).

[29] M. Gerster, M. Rizzi, F. Tschirsich, P. Silvi, R. Fazio, and S. Montangero, New J. Phys. **18**, 015015 (2016).

[30] E. V. H. Doggen, G. Lemarié, S. Capponi, and N. Laflorencie, Phys. Rev. B **96**, 180202 (2017).

[31] A. Erez and Y. Meir, Phys. Rev. Lett. **111**, 187002 (2013).

[32] I. Maccari, L. Benfatto, and C. Castellani, Phys. Rev. B **96**, 060508 (2017).

[33] I. Maccari, L. Benfatto, and C. Castellani, Condens. Matter **3**, 8 (2018).

[34] V. L. Berezinskii, Zh. Eksp. Teor. Fiz. **61**, 1144 (1972) [Sov. Phys. JETP **34**, 610 (1972)].

[35] J. M. Kosterlitz and D. J. Thouless, J. Phys. C **6**, 1181 (1973).

[36] J. Kosterlitz, J. Phys. C **7**, 1046 (1974).

[37] L. Benfatto, C. Castellani, and T. Giamarchi, in *40 Years of Berezinskii–Kosterlitz–Thouless Theory* (World Scientific, Singapore, 2013), pp. 161–199.

[38] V. N. Popov, *Functional Integrals in Quantum Field Theory and Statistical Physics*, Vol. 8 (Reidel, Dordrecht, 1983).

[39] D. P. Landau and K. Binder, *A Guide to Monte Carlo Simulations in Statistical Physics* (Cambridge University Press, Cambridge, 2005).

[40] S. Andergassen, T. Enss, V. Meden, W. Metzner, U. Schollwöck, and K. Schönhammer, Phys. Rev. B **70**, 075102 (2004).

[41] T. Enss, V. Meden, S. Andergassen, X. Barnabé-Thériault, W. Metzner, and K. Schönhammer, Phys. Rev. B **71**, 155401 (2005).

[42] C. Rylands and N. Andrei, Phys. Rev. B **94**, 115142 (2016).

[43] M. Cazalilla, J. Phys. B **37**, S1 (2004).

[44] D. Ariosa and H. Beck, Phys. Rev. B **43**, 344 (1991).

[45] Y.-D. Hsieh, Y.-J. Kao, and A. W. Sandvik, J. Stat. Mech. (2013) P09001.